Supporting Information

Phenanthrene-Based Deep-blue Fluorophores with Balanced Carrier Transport Ability for High-Performance OLEDs with CIE_y < 0.04

Shiyan Guo [a], Xin Jin [a], Daqing Zhang [a], Haitao Zhou [c], Guoliang Wang [b], Yanqin Miao [*b], Jinhai Huang [*c], Zhiyun Zhang [a], Hua Wang [d], Jianhua Su [*a]

[a]*Key Laboratory for Advanced Materials and Institute of Fine Chemicals, East China University of Science & Technology, Shanghai 200237, China*

[b]*Key Laboratory of Interface Science and Engineering in Advanced Materials Taiyuan University of Technology, Taiyuan 030024, China*

[c]*Shanghai Taoe Chemical Technology Co., Ltd, Shanghai 200030, China*

[d]*College of Textile Engineering, Taiyuan University of Technology, Jin Zhong, 030600, China*

Corresponding E-mails: bbsjh@ecust.edu.cn (Jianhua Su); miaoyanqin@tyut.edu.cn (Yanqin Miao); dele12@163.com (Jinhai Huang)

Content

General Information 4

Devices Fabrication 5

Experimental section 6

Additional data 9

Fig. S1 The DSC curves of Cz1, Cz2 and TPA1. 9

Fig. S2 Electronic absorption spectrum of Cz2. Respective contribution curves corresponding to excitations from HOMO to various unoccupied molecular orbitals are plotted, only the excitations with *f* larger than 0.02 and HOMO→LUMO are taken into account. The *f* of HOMO→LUMO of 0.0062 is too small to the contribution to the first absorption peak. 9

Fig. S3 Electronic absorption spectrum of TPA1. Respective contribution curves corresponding to excitations from HOMO to various unoccupied molecular orbitals are plotted, only the excitations with *f* larger than 0.015 are taken into account. 10

Fig. S4 (a) Optimized singlet state geometries and (b) spatial distributions of the HOMO and LUMO levels for Cz1, Cz2 and TPA1 in singlet state. 10

Fig. S5 The UV-Vis and PL curves of Cz1 in various polarities solvents. 11

Fig. S6 The UV-Vis and PL curves of Cz2 in various polarities solvents. 11

Fig. S7 The UV-Vis and PL curves of TPA1 in various polarities solvents. 11

Fig. S8 The PL curves of Cz1, Cz2 and TPA1 in PMMA matrix. 12

Fig. S9 (a) The PL curves and (b) the low-temperature phosphorescence curves of Cz1, Cz2 and TPA1 in neat film. 12

Fig. S10 The PL emission of TPA1 doped in mCP with various doping concentrations. 12

Fig. S11 Electric field-dependent mobility of hole-only and electron-only devices of Cz1 (a) and Cz2 (b). 13

Fig. S12 (a)The CE and PE versus luminance of B1, B2 and B3. (b)The EL of B1 at 4-8V. (c)The EL of B2 at 4-9V. (d)The EL of B3 at 4-8V. 13

Table S1 The performance of some deep-blue emitters with CIE_y < 0.10 which have been reported. 13

Fig. S13 (a)The device structure and energy diagram. (b)The EL emissions of B4, B5, B6 and B7. (c)The CE and PE versus luminance of B4, B5, B6 and B7. 15

Fig. S14 (a)The CE and PE versus luminance of G1, G2 and G3. (b)The EL of G1 at 4-8V. (c)The EL of G2 at 4-9V. (d)The EL of G3 at 4-8V. 16

Table S2 The performance of some reported green PhOLEDs.....16

Fig. S15 The ^{1}H and ^{13}C of Inter 1.....18

Fig. S16 The MS of Inter 1.....18

Fig. S17 The ^{1}H and ^{13}C of Cz1.....19

Fig. S18 The MS of Cz1.....20

Fig. S19 The ^{1}H and ^{13}C of Cz2.....21

Fig. S20 The MS of Cz2.....21

Fig. S21 The ^{1}H and ^{13}C of TPA1. 22

Fig. S22 The MS of TPA1.....23

Reference 24

General Information

All other chemicals and reagents were purchased from *Shanghai Haohong Scientific Co., Ltd* and used as received without further purification. ^{1}H and ^{13}C NMR spectra were measured on a Bruker AM 400 spectrometers in appropriated deuterated solution at room temperature. High-resolution mass spectra (HRMS) were recorded on a XEVO G2 TOF spectrometer. UV-vis absorption spectra were measured on an Agilent spectrophotometer. Photoluminescence (PL) spectra were recorded on a Horiba FluoroMax plusspectrofluorometer. Thermogravimetric analysis (TGA) was carried on a thermal gravimetric analyzer (SHIMADZU TGA-50/50H instrument) under dry nitrogen at a heating rate of 20 ^{o}C/min from 50 ^{o}C to 600 ^{o}C. Differential scanning calorimetry (DSC) was run on a SHIMADZU DSC-60Plus instrument. DSC tests were carried out under dry nitrogen, and there were 4 temperature controlling process: a) 30→250 ^{o}C (20 ^{o}C/min); b) 250→30 ^{o}C (20 ^{o}C/min); c) 30 ^{o}C→250 ^{o}C (20 ^{o}C/min); d) 250→30 ^{o}C (20 ^{o}C/min). Cyclic voltammograms were obtained in dichloromethane containing 0.1 M tetrabutylammonium hexafluorophosphate for oxidation processes, respectively, with a scan rate of 50 mV/s, using a platinum wire as the auxiliary electrode, a glass carbon disk as the working electrode and a saturated calomel (Hg/Hg_2Cl_2) as the reference electrode. The geometry optimization of the ground state and the HOMO/LUMO energy levels were realized by DFT method at B3LYP/6-31G(d, p) level. The electronic absorption spectrum were realized by TD-DFT method with B3LYP functional and 6-31G(d, p) basis set. The electron and hole analyses of singlet excited state were calculated at TD-CAM-B3LYP-D3(BJ)/6-31+g(d,p) level.

Devices Fabrication

The glass substrates precoated with a 90-nm layer of indium tin oxide (ITO) with a sheet resistance of 15 to 20 ohms per square were successively cleaned in ultrasonic bath of acetone, isopropanol, detergent, and deionized water, respectively, taking 10 min for each step. Before the fabrication processes, to improve the hole injection ability of ITO, the substrates were treated by ultraviolet-ozone for 10 min. The vacuum-deposited OLEDs were fabricated under a pressure of $<5\times10^{-4}$ Pa in a vacuum deposition system. The deposition rates and film thicknesses were monitored by calibrated crystal quartz sensors. Organic materials, LiF, and Al were deposited at rates of 1 to 1.5 Å/s, 0.3 Å/s, and 3-5 Å/s, respectively. The effective emitting area of the device was 9 mm^2, determined by the overlap between anode and cathode.

The EL spectra and CIE coordinates of all OLEDs were measured by a computer controlled PR-655 spectra scan spectrometer. The current density-voltage-luminance characteristics, current efficiency, and power efficiency were recorded by a computer-controlled Keithley 2400 source integrated with a BM-70A luminance meter. The EQE was calculated from the current density-voltage-luminance curve and spectra data. All samples were immediately characterized after thin films deposition without encapsulation in ambient atmosphere at room temperature.

Experimental section

Synthesis and characterization

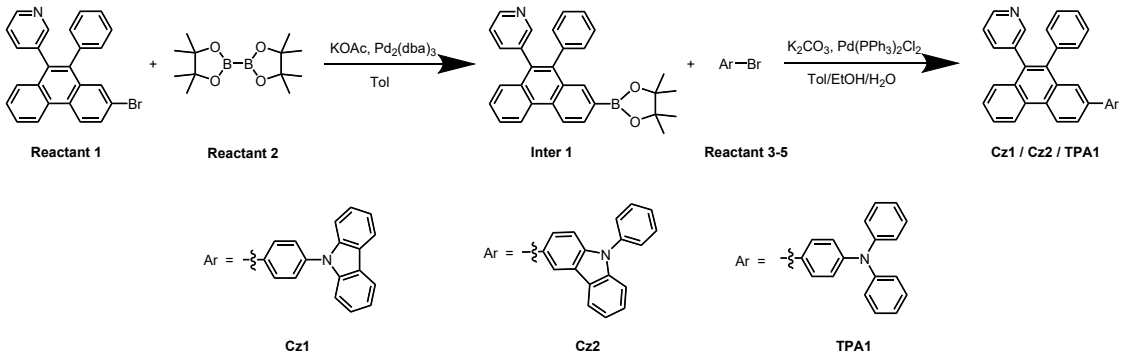

3-(10-phenyl-2-(4,4,5,5-tetramethyl-1,3,2-dioxaborolan-2-yl)phenanthren-9-yl)pyridine (**Inter 1**)

Inter 1 was synthesized by Suzuki coupling reaction. The mixture of **Reactant 1** (4.00 g, 9.78 mmol), **Reactant 2** (2.99 g, 11.74 mmol), KOAc (2.88 g, 29.34 mmol) and $Pd_2(dba)_3$ (0.4 g, 10 wt%) were dried 2 h under vacuum. After addition of ultradry Tol (50 mL), the reaction mixture was refluxed 4 h under N_2 and then cooled to room temperature. The resulted solution was purified by a silica column to separate catalyst and inorganic salt. The organic solvent was concentrated under rotary evaporation and white solid was precipitated. The product was obtained following filtered, washed and dried, 3.58 g, yield of 80%. ^{1}H NMR (400 MHz, $CDCl_3$) δ: 8.86 (d, J = 8.3 Hz, 1H), 8.80 (d, J = 8.3 Hz, 1H), 8.52-8.36 (m, 2H), 8.15-7.98 (m, 2H), 7.69 (ddd, J = 8.4, 6.8, 1.4 Hz, 1H), 7.59-7.41 (m, 3H), 7.31-7.09 (m, 6H), 1.31 (s, 12H). ^{13}C NMR (101 MHz, $CDCl_3$) δ: 151.21, 147.37, 139.01, 138.82, 138.65, 135.83, 135.11, 133.15, 132.43, 132.31, 131.89, 131.23, 130.97, 130.79, 129.94, 128.14, 127.74, 127.38, 127.15,

126.93, 126.72, 123.18, 122.81, 121.75, 83.92, 24.86. HRMS (ESI, *m/z*): $[M+H]^+$ calculated for $C_{31}H_{28}BNO_2$, 458.2291, found 458.2296.

9-(4-(10-phenyl-9-(pyridin-3-yl)phenanthren-2-yl)phenyl)-9*H*-carbazole (**Cz1**)

Inert 1 (1.00 g, 2.19 mmol), 9-(4-bromophenyl)-9*H*-carbazole (**Reactant 3**) (0.70 g, 2.19 mmol), K_2CO_3 (0.9 g, 6.56 mmol) and $Pd(PPh_3)_2Cl_2$ (0.1 g, 10 wt%) were dissolved in Tol (20 mL), EtOH (10 mL) and H_2O (10 mL). Stopped the reaction after refluxed 4 h under N_2 and cooled to room temperature. Water was removed by separatory funnel and the organic layer was filtered with silica gel column. The filter liquor was concentrated to 5 mL and white product was precipitated after addition of EtOH (10 mL). The ulteriorly extracted by filtration and the filter cake was washed by Tol and EtOH, 1.13 g dried product was gained, yield of 90%. ^{1}H NMR (400 MHz, $CDCl_3$) δ: 8.94 (d, J = 8.8 Hz, 1H), 8.88 (d, J = 8.4 Hz, 1H), 8.47 (dd, J = 4.8, 1.8 Hz, 2H), 8.14 (dd, J = 7.8, 1.2 Hz, 2H), 8.04 (dd, J = 8.6, 2.0 Hz, 1H), 7.89 (d, J = 2.0 Hz, 1H), 7.81-7.70 (m, 3H), 7.64-7.58 (m, 2H), 7.58-7.48 (m, 3H), 7.43 (dtd, J = 15.2, 8.3, 1.2 Hz, 4H), 7.35-7.18 (m, 8H). ^{13}C NMR (101 MHz, $CDCl_3$) δ: 151.57, 147.97, 140.80, 139.79, 138.76, 138.63, 138.47, 138.34, 137.06, 135.44, 134.08, 132.10, 131.62, 131.15, 130.87, 129.92, 129.65, 128.68, 128.35, 127.96, 127.41, 127.15, 127.00, 126.01, 123.50, 123.46, 122.86, 122.73, 120.36, 120.05, 109.86. HRMS (ESI, *m/z*): $[M+H]^+$ calculated for $C_{43}H_{28}N_2$, 573.2331, found 573.2333.

9-phenyl-3-(10-phenyl-9-(pyridin-3-yl)phenanthren-2-yl)-9*H*-carbazole (**Cz2**)

The synthesis process of **Cz2** is same as **Cz1**, 3-bromo-9-phenyl-9*H*-carbazole (**Reactant 4**) replaces **Reactant 3**, white solid (1.15 g, 92%). ^{1}H NMR (400 MHz,

$CDCl_3$) δ: 8.91 (d, J = 8.6 Hz, 1H), 8.86 (d, J = 8.4 Hz, 1H), 8.47 (dt, J = 6.6, 2.0 Hz, 2H), 8.32 (d, J = 1.6 Hz, 1H), 8.20-8.13 (m, 1H), 8.09 (dd, J = 8.6, 2.0 Hz, 1H), 7.87 (d, J = 1.8 Hz, 1H), 7.71 (ddd, J = 8.4, 6.4, 1.8 Hz, 1H), 7.64-7.38 (m, 12H), 7.34-7.17 (m, 7H). ^{13}C NMR (101 MHz, $CDCl_3$) δ: 151.43, 147.69, 141.39, 140.49, 140.30, 138.87, 138.76, 138.58, 137.57, 135.70, 133.61, 132.98, 132.14, 131.40, 131.15, 130.87, 130.08, 129.95, 128.91, 128.26, 127.85, 127.61, 127.30, 127.08, 126.86, 126.83, 126.54, 126.25, 126.00, 125.64, 123.92, 123.40, 123.22, 122.78, 120.41, 120.14, 119.01, 110.17, 109.98. HRMS (ESI, *m/z*): $[M+H]^+$ calculated for $C_{43}H_{28}N_2$, 573.2331, found 573.2332.

N,*N*-diphenyl-4-(10-phenyl-9-(pyridin-3-yl)phenanthren-2-yl)aniline (**TPA1**)

The synthesis process of **TPA1** is same as **Cz1**, 4-bromo-*N*,*N*-diphenylaniline (**Reactant 5**) replaces **Reactant 3**, white solid (1.06 g, 85%). ^{1}H NMR (400 MHz, $CDCl_3$) δ: 8.84 (t, J = 8.6 Hz, 2H), 8.46 (t, J = 2.8 Hz, 2H), 7.94 (dd, J = 8.6, 2.0 Hz, 1H), 7.75 (d, J = 1.9 Hz, 1H), 7.70 (ddd, J = 8.2, 6.6, 1.4 Hz, 1H), 7.57-7.49 (m, 2H), 7.49-7.39 (m, 3H), 7.27 (d, J = 2.0 Hz, 3H), 7.23-7.13 (m, 4H), 7.15-7.06 (m, 6H), 7.03 (td, J = 7.3, 1.3 Hz, 2H). ^{13}C NMR (101 MHz, $CDCl_3$) δ: 151.42, 147.73, 147.58, 147.44, 138.83, 138.81, 138.67, 138.51, 135.61, 134.30, 133.67, 132.04, 131.40, 131.11, 130.83, 129.99, 129.34, 129.04, 128.25, 127.89, 127.84, 127.29, 127.05, 126.87, 125.76, 125.22, 124.60, 123.68, 123.21, 123.11, 122.75. HRMS (ESI, *m/z*): $[M+H]^+$ calculated for $C_{43}H_{30}N_2$, 575.2487, found 575.2489.

Additional data

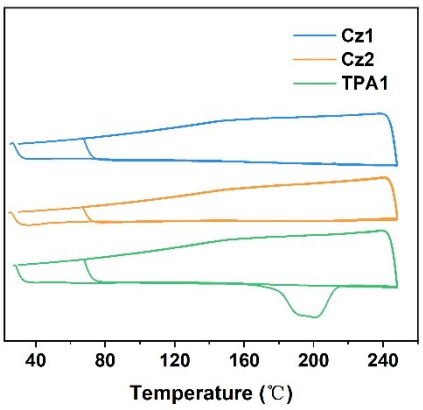

Fig. S1 The DSC curves of **Cz1, Cz2** and **TPA1.**

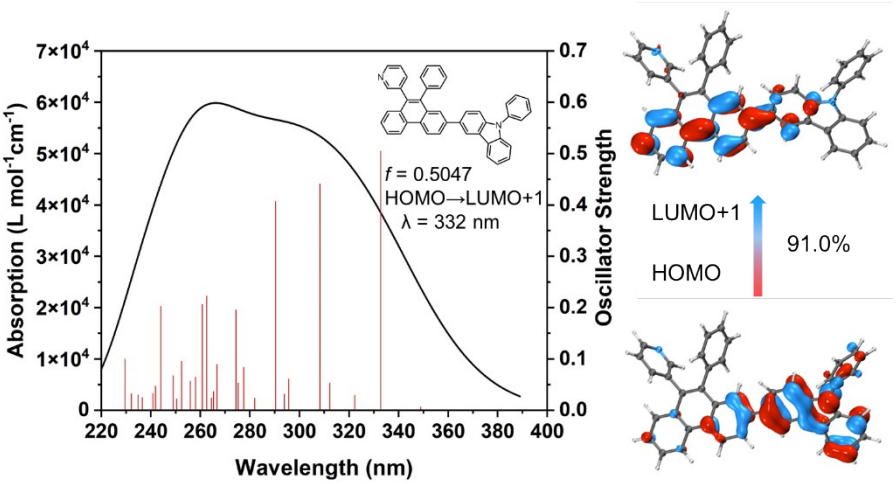

Fig. S2 Electronic absorption spectrum of **Cz2**. Respective contribution curves corresponding to excitations from HOMO to various unoccupied molecular orbitals are plotted, only the excitations with *f* larger than 0.02 and HOMO→LUMO are taken into account. The *f* of HOMO→LUMO of 0.0062 is too small to the contribution to the first absorption peak.

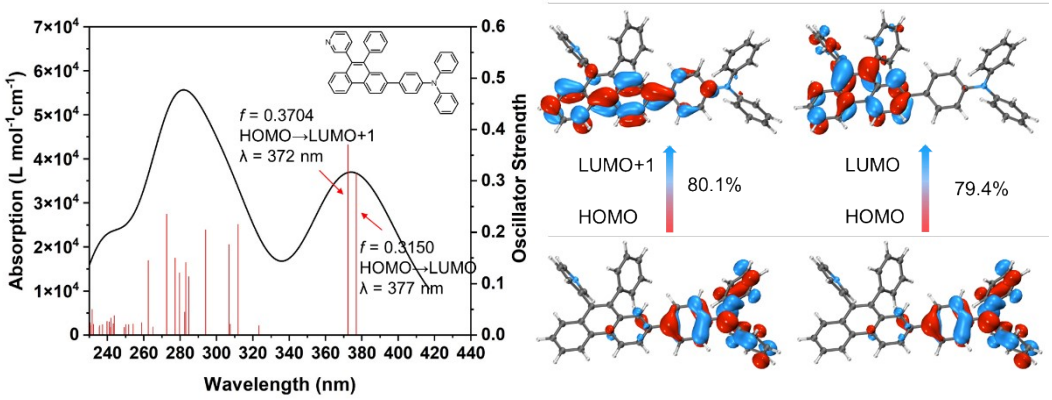

Fig. S3 Electronic absorption spectrum of **TPA1**. Respective contribution curves corresponding to excitations from HOMO to various unoccupied molecular orbitals are plotted, only the excitations with *f* larger than 0.015 are taken into account.

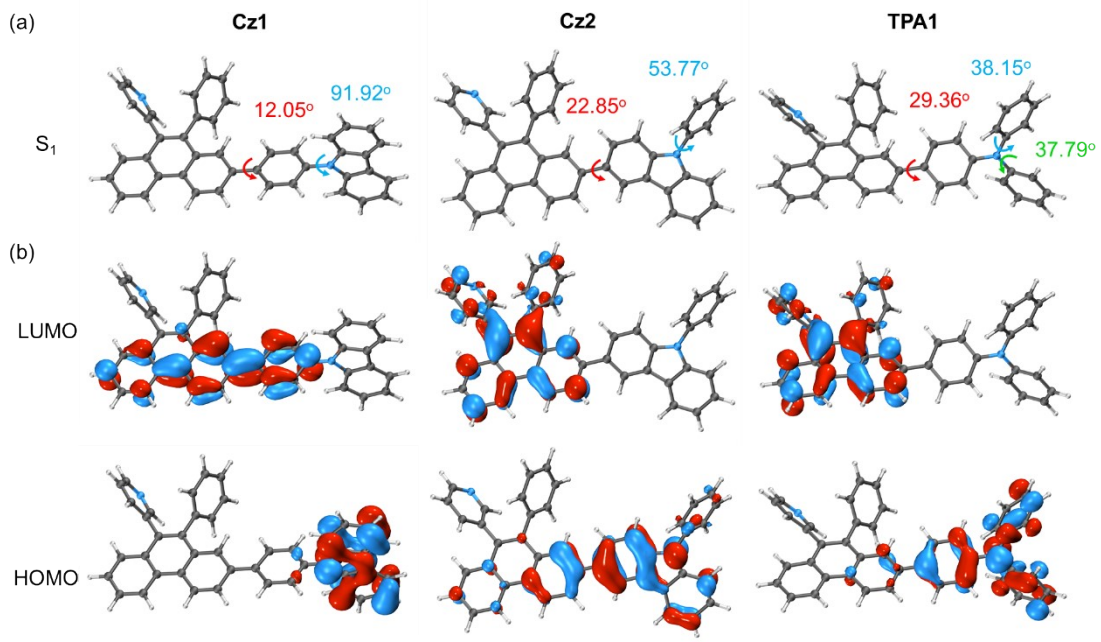

Fig. S4 (a) Optimized singlet state geometries and (b) spatial distributions of the HOMO and LUMO levels for **Cz1**, **Cz2** and **TPA1** in singlet state**.**

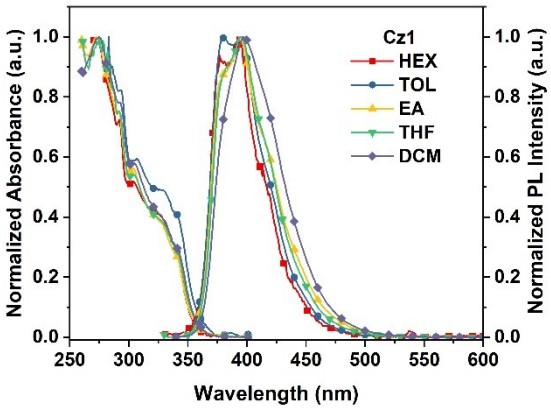

Fig. S5 The UV-Vis and PL curves of **Cz1** in various polarities solvents.

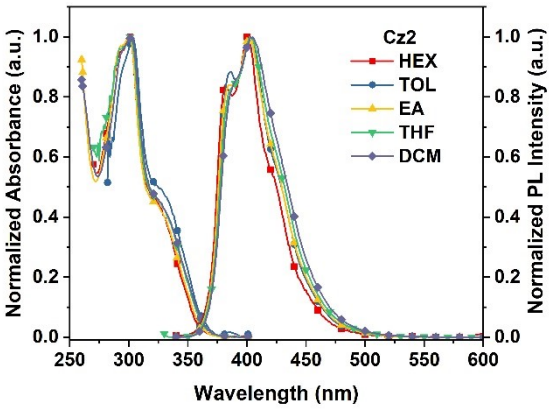

Fig. S6 The UV-Vis and PL curves of **Cz2** in various polarities solvents.

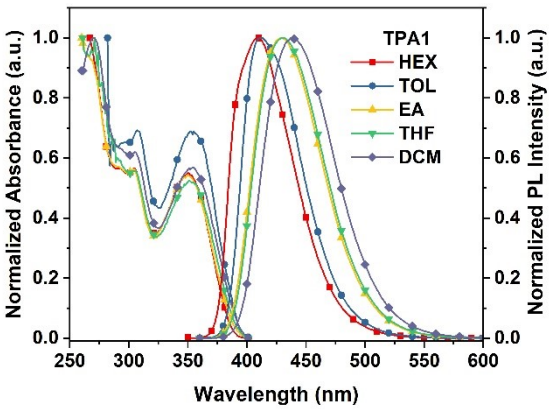

Fig. S7 The UV-Vis and PL curves of **TPA1** in various polarities solvents.

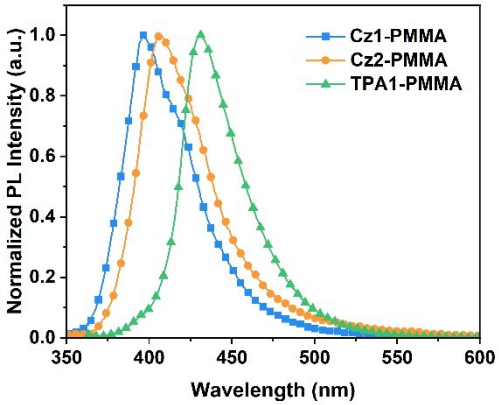

Fig. S8 The PL curves of **Cz1**, **Cz2** and **TPA1** in PMMA matrix.

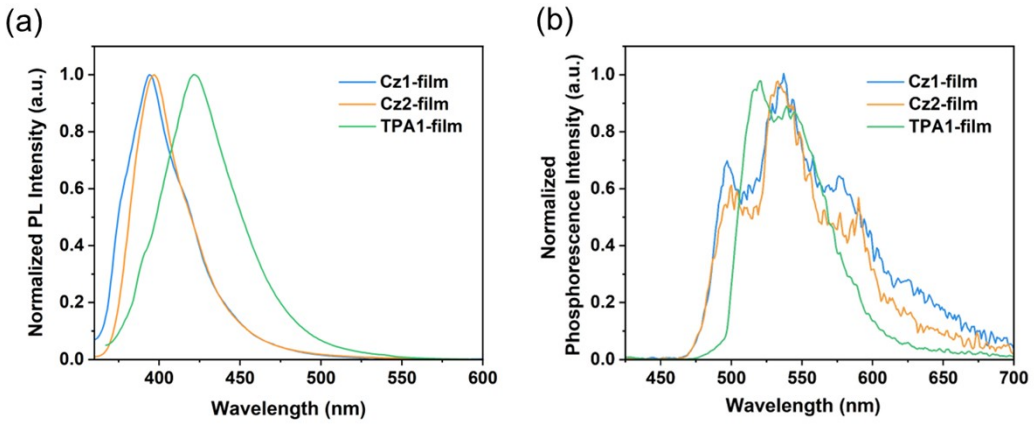

Fig. S9 (a) The PL curves and (b) the low-temperature phosphorescence curves of **Cz1**, **Cz2** and **TPA1** in neat film.

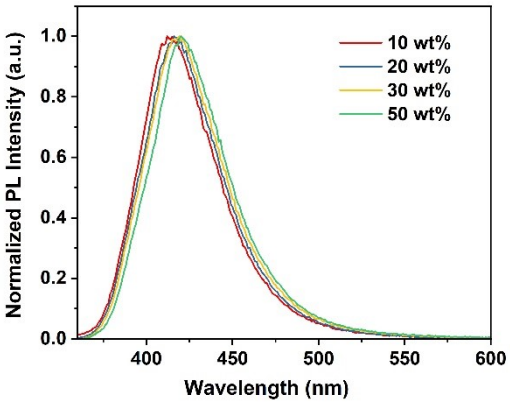

Fig. S10 The PL emission of **TPA1** doped in mCP with various doping concentrations.

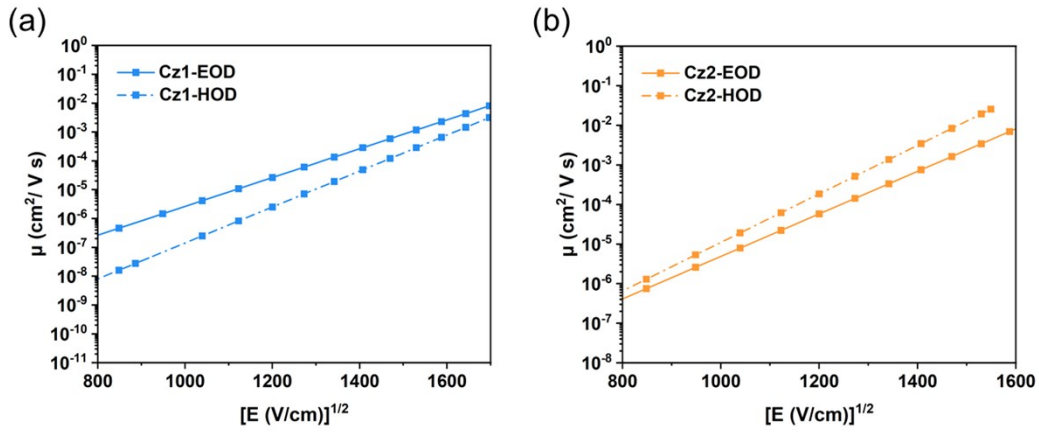

Fig. S11 Electric field-dependent mobility of hole-only and electron-only devices of **Cz1** (a) and **Cz2** (b).

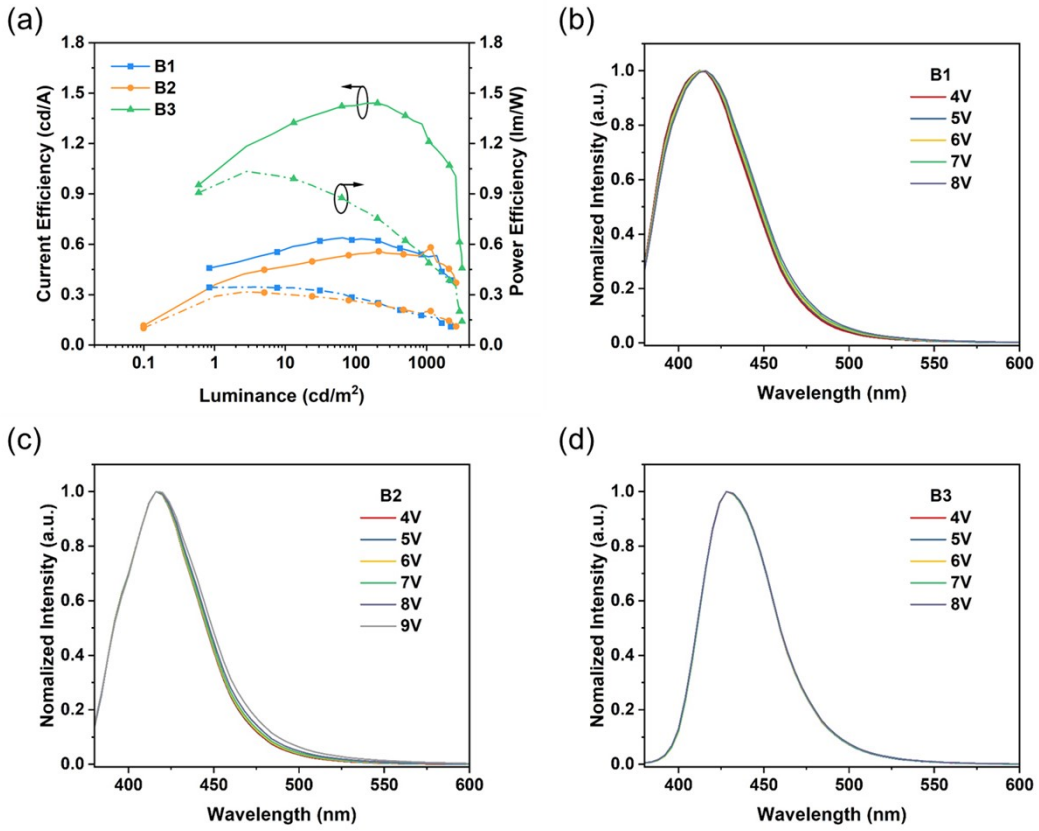

Fig. S12 (a)The CE and PE versus luminance of B1, B2 and B3. (b)The EL of B1 at 4-8V. (c)The EL of B2 at 4-9V. (d)The EL of B3 at 4-8V.

Table S1 The performance of some deep-blue emitters with CIE_y < 0.10 which have been reported.

Devices	λ_{EL} (nm)	V_{on}[a] (V)	L_{max} (cd/m^2)	EQE_{max} (%)	CE_{max} (cd/A)	PE_{max} (lm/W)	CIE[b] (x, y)	reference
TPA1	430	3.4	3160	4.36	1.44	1.03	(0.156, 0.037)	This work
PIPD-MP-DPA	428	2.4	4158	4.40	2.40	2.50	(0.154, 0.078)	Ref. 1
PIPD-MP-DPAC	418	3.1	1617	1.90	1.00	0.90	(0.159, 0.092)	Ref. 1
TBDNPA	444	3.0	6940	5.17	2.63	1.96	(0.149, 0.086)	Ref. 2
TBMFA	444	3.2	2190	3.58	1.79	1.41	(0.151, 0.085)	Ref. 2
BBPA	432	3.2	/	5.28	/	/	(0.150, 0.060)	Ref. 3
DMPA	436	3.3	/	4.97	/	/	(0.160, 0.080)	Ref. 3
F-2CzB	404	3.2	2775	4.43	/	/	(0.162, 0.028)	Ref. 4
mTPE-PPI	452	3.9	3095	2.30	1.83	1.48	(0.150, 0.090)	Ref. 5
PPi-Pid	450	2.90	17100	4.95	3.96	/	(0.150, 0.092)	Ref. 6
PPi-Xid	445	3.30	9163	4.21	2.46	/	(0.152, 0.057)	Ref. 6
PPi-Mid	440	3.10	9165	4.90	2.70	/	(0.154, 0.058)	Ref. 6
DFPBI	435	3.0	2690	4.18	1.48	/	(0.154,0.042)	Ref. 7
TPA-PIM	420	/	4510	3.28	1.14	0.79	(0.161, 0.046)	Ref. 8

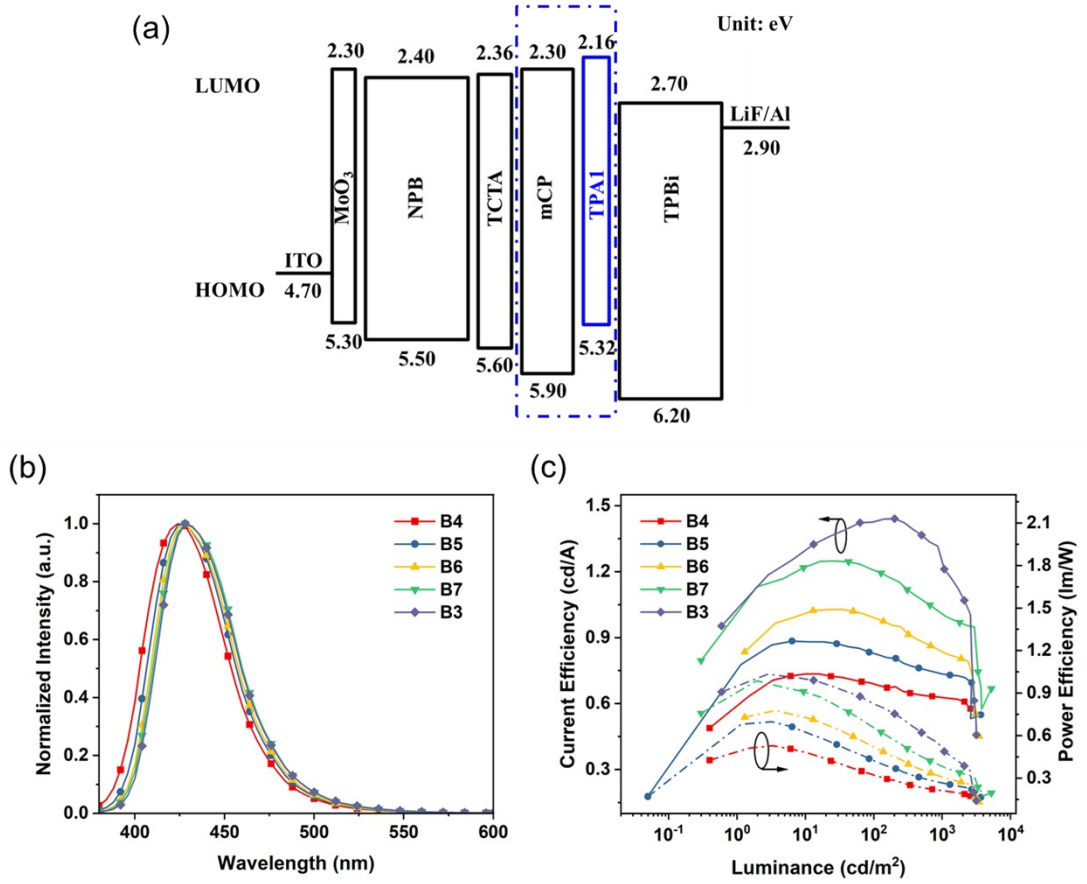

Fig. S13 (a)The device structure and energy diagram. (b)The EL emissions of B4, B5, B6 and B7. (c)The CE and PE versus luminance of B4, B5, B6 and B7.

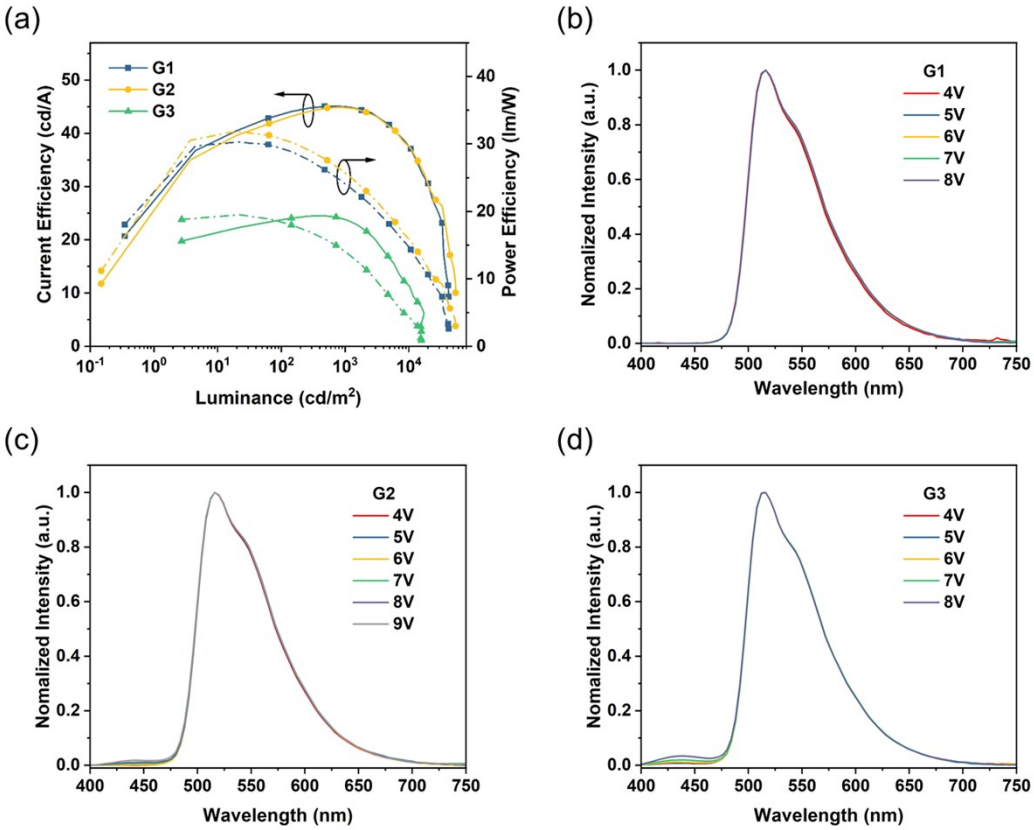

Fig. S14 (a)The CE and PE versus luminance of G1, G2 and G3. (b)The EL of G1 at 4-8V. (c)The EL of G2 at 4-9V. (d)The EL of G3 at 4-8V.

Table S2 The performance of some reported green PhOLEDs.

EML	λ_{EL} (nm)	V_{on}[a] (V)	L_{max} (cd/m^2)	EQE_{max} (%)	CE_{max} (cd/A)	PE_{max} (lm/W)	reference
Cz1: Ir(ppy)$_3$	516	3.7	42260	12.9	45.1	30.3	This work
Cz2: Ir(ppy)$_3$	516	3.5	54380	12.7	44.9	31.9	This work
CzTrz: Ir(ppy)$_3$	515	3.5	30280	15.5	54.3	38.1	Ref. 9
BCz2: Ir(ppy)$_3$	510	3.8	35050	11.8	40.6	30.3	Ref. 9
CNPhCz: Ir(ppy)$_2$acac	/	3.2	22 080	24.4	88.0	86.0	Ref. 10
DCNPhCz: Ir(ppy)$_2$acac	/	3.7	14 000	21.0	59.5	53.6	Ref. 10

PymCP: $Ir(ppy)_3$	/	3.6	50 524	18.7	65.8	43.9	Ref. 11
***m*-PyPOmCP**: $Ir(ppy)_3$	/	2.7	61 140	24.4	88.5	92.6	Ref. 11
3,6-DCP: $Ir(ppy)_2(acac)$	/	4.2	/	12.1	44.0	13.1	Ref. 12
2,9-DCBQ: $Ir(ppy)_2(acac)$	/	3.5	/	9.8	35.5	12.3	Ref. 12
3,9-DCBQ: $Ir(ppy)_2(acac)$	/	3.0	/	14.3	48.5	20.6	Ref. 12
***m*-PyCNmCP**: $Ir(ppy)_3$	/	2.0	45510	18.4	68.2	101.4	Ref. 13
OCI: $Ir(ppy)_3$	/	2.7	61190	14.11	49.43	57.49	Ref. 14
OCT: $Ir(ppy)_3$	/	2.7	97940	15.57	52.81	46.71	Ref. 14
TPA-1: $Ir(ppy)_3$	527	2.7	46000	9.2	34.4	35.4	Ref. 15
CBZ-1: $Ir(ppy)_3$	530	2.3	10000	12.6	47.1	62.1	Ref. 15

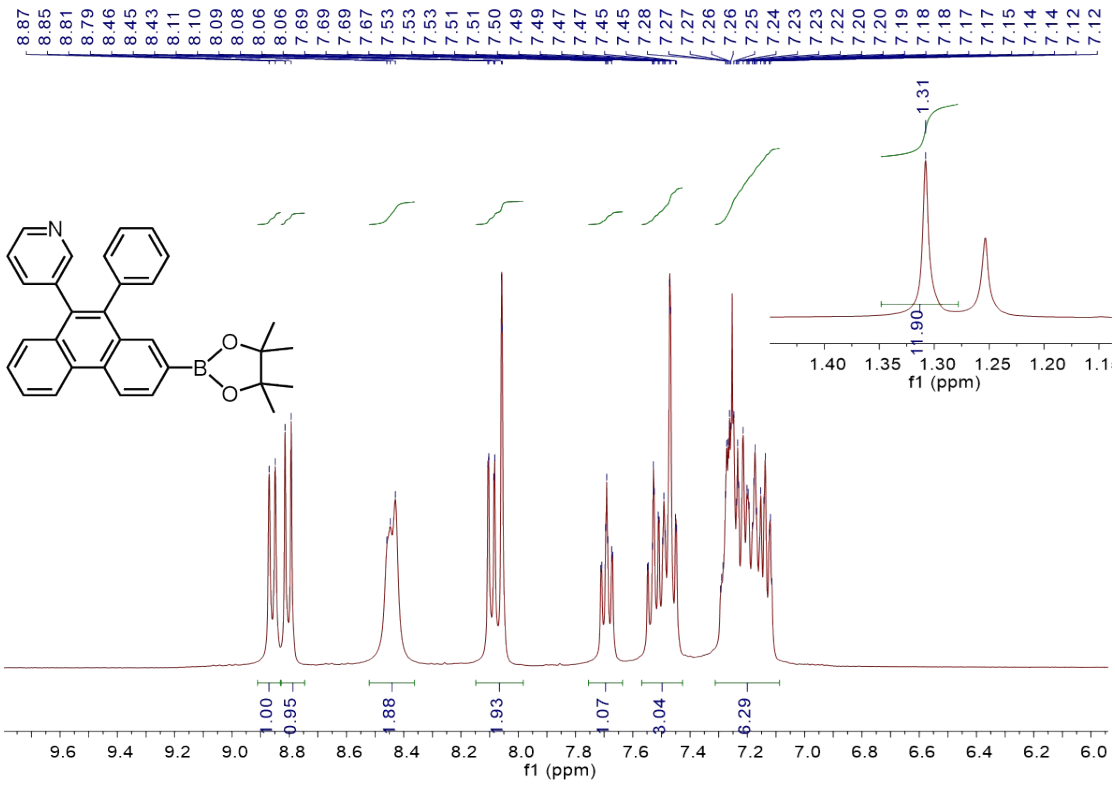

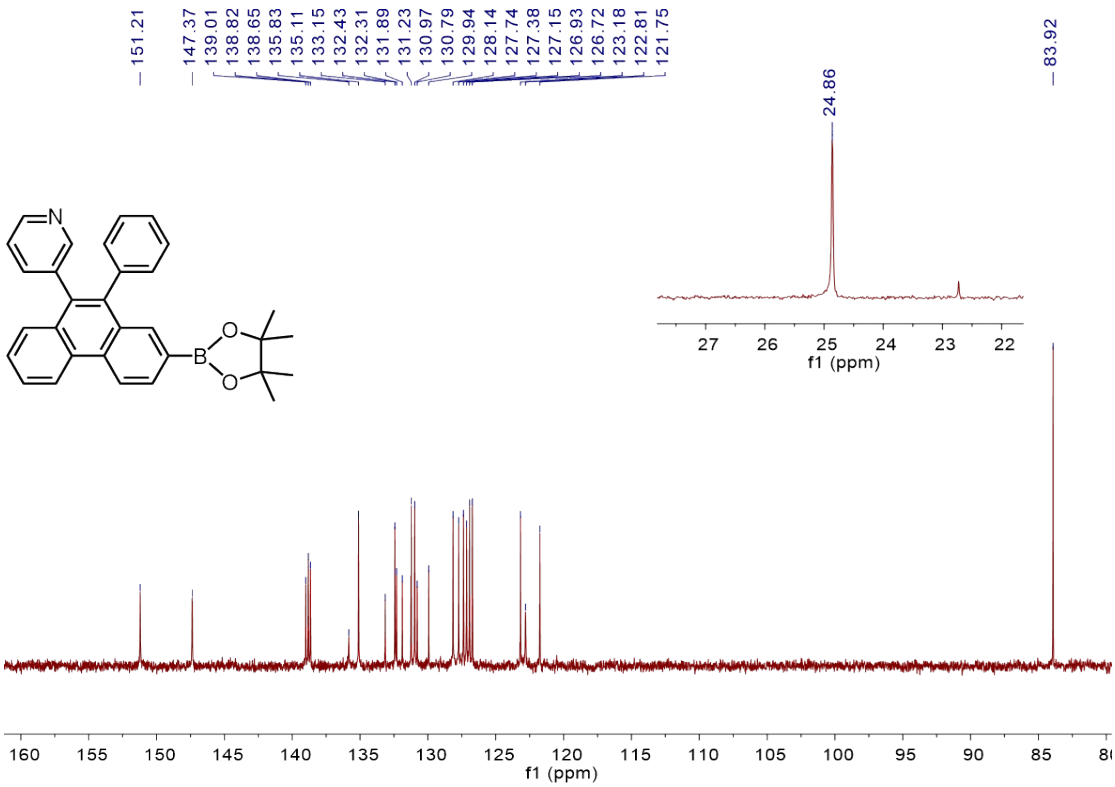

Fig. S15 The ^{1}H and ^{13}C of Inter 1.

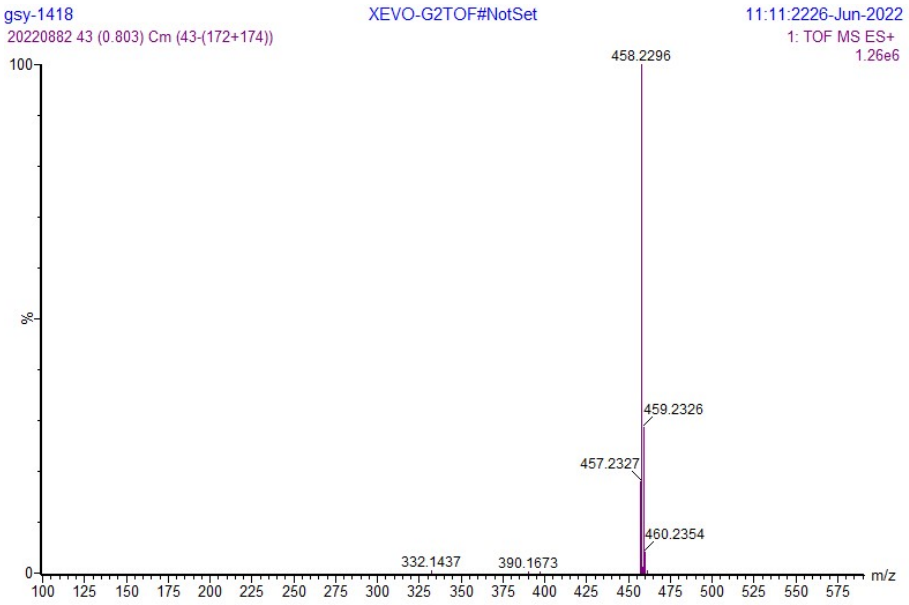

Fig. S16 The MS of Inter 1.

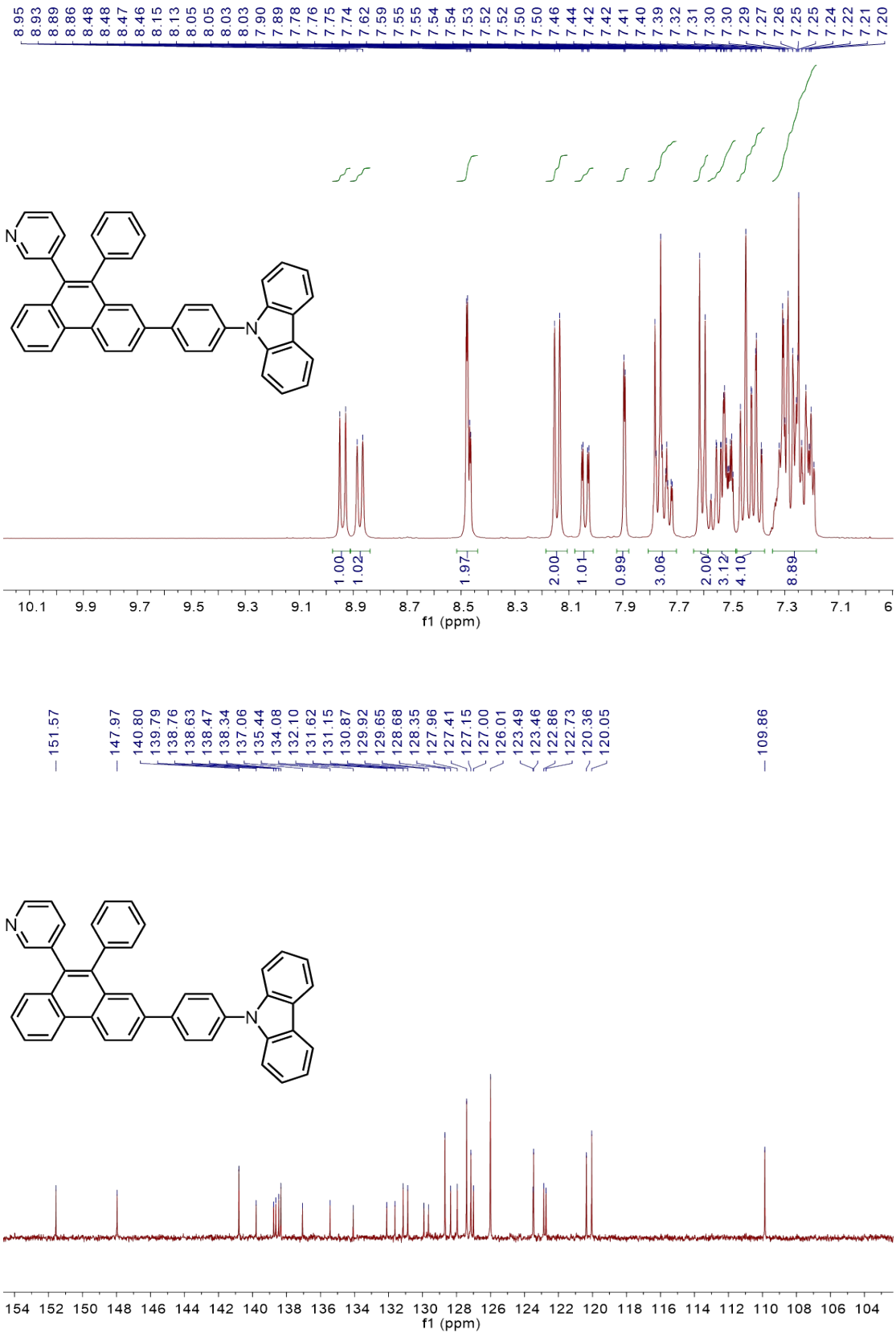

Fig. S17 The ^{1}H and ^{13}C of Cz1.

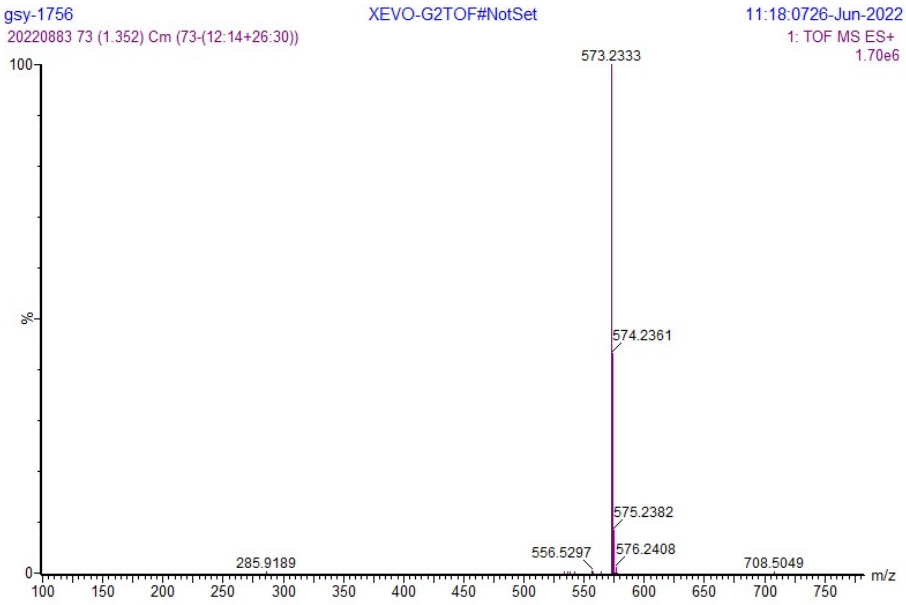

Fig. S18 The MS of Cz1.

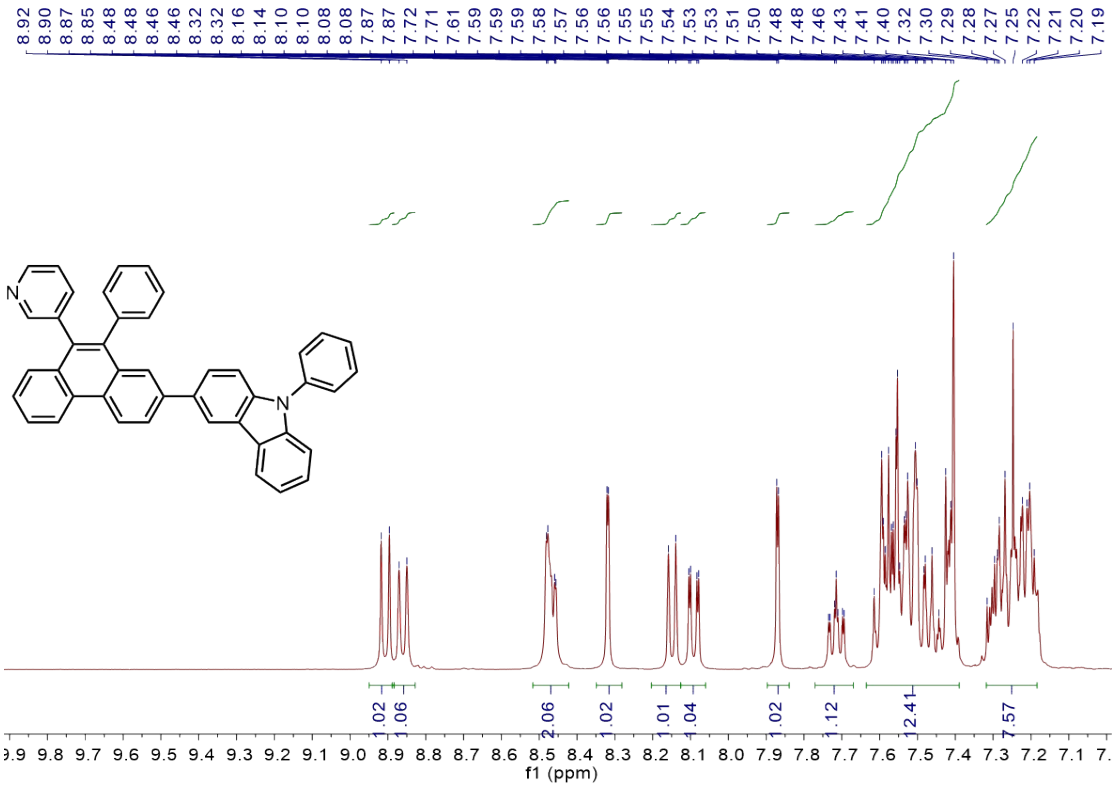

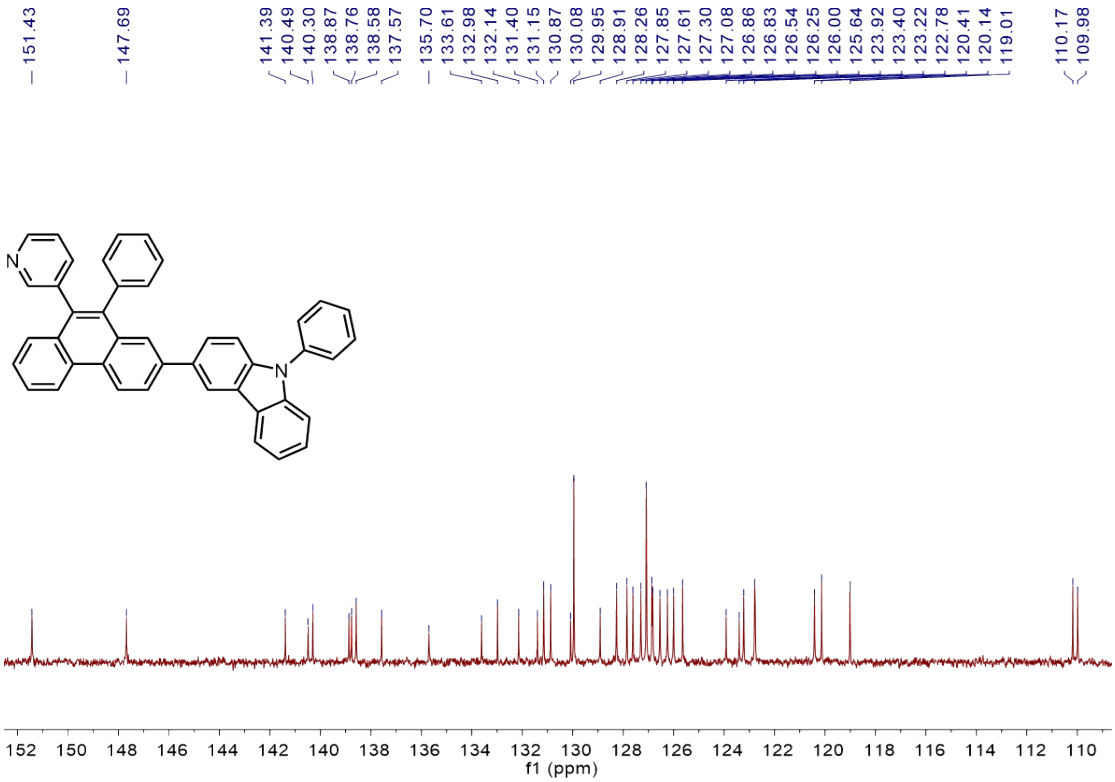

Fig. S19 The ^{1}H and ^{13}C of Cz2.

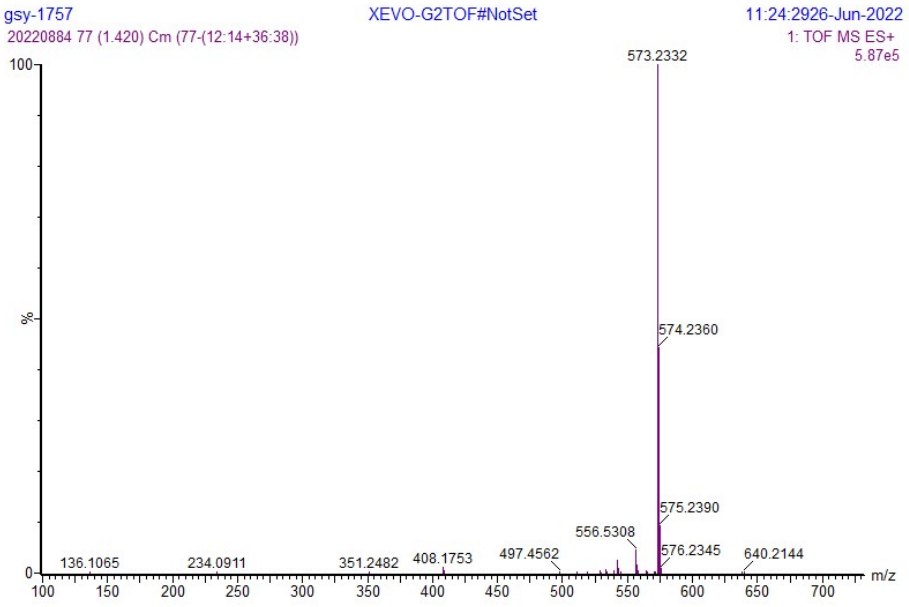

Fig. S20 The MS of Cz2.

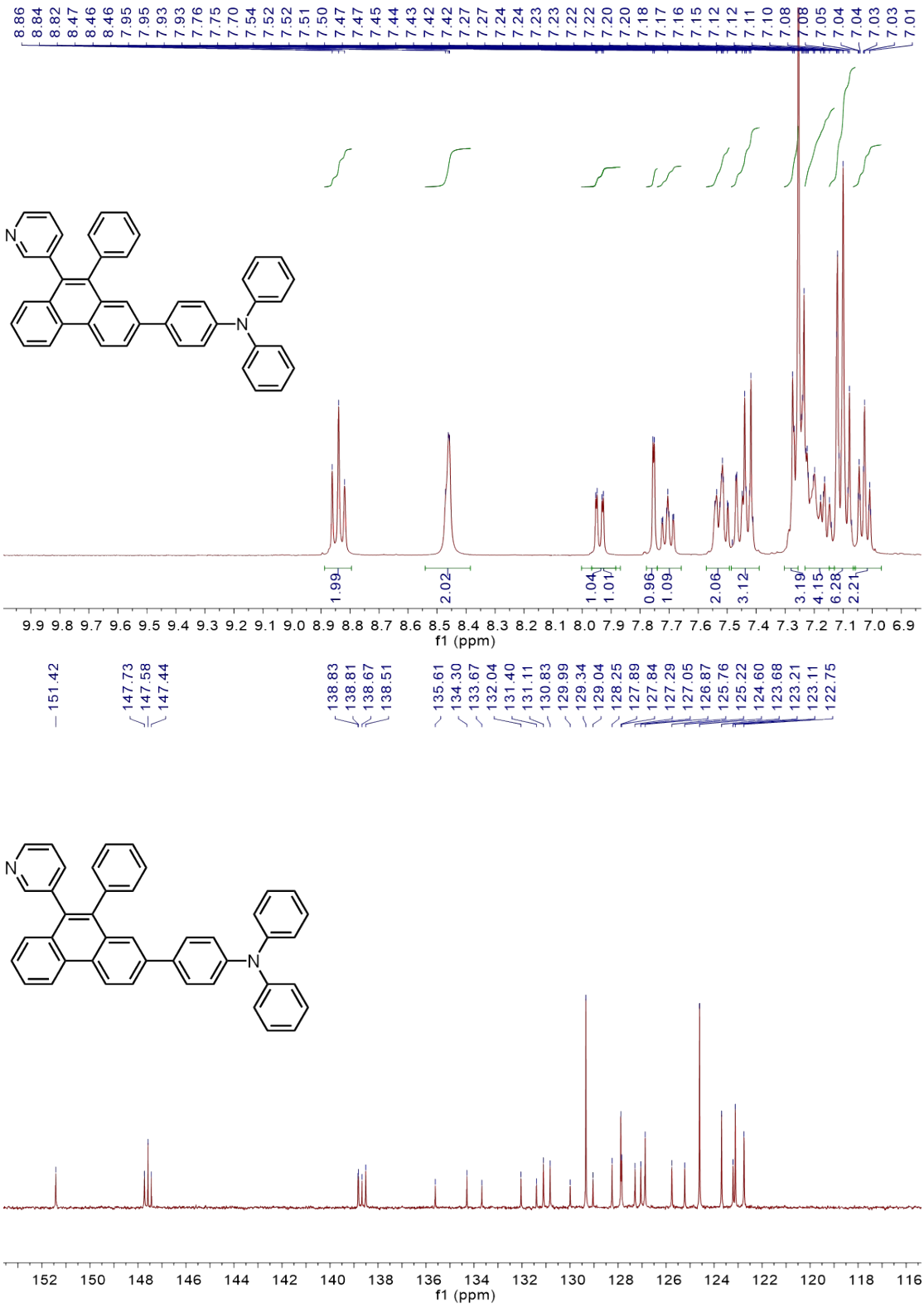

Fig. S21 The ^{1}H and ^{13}C of TPA1.

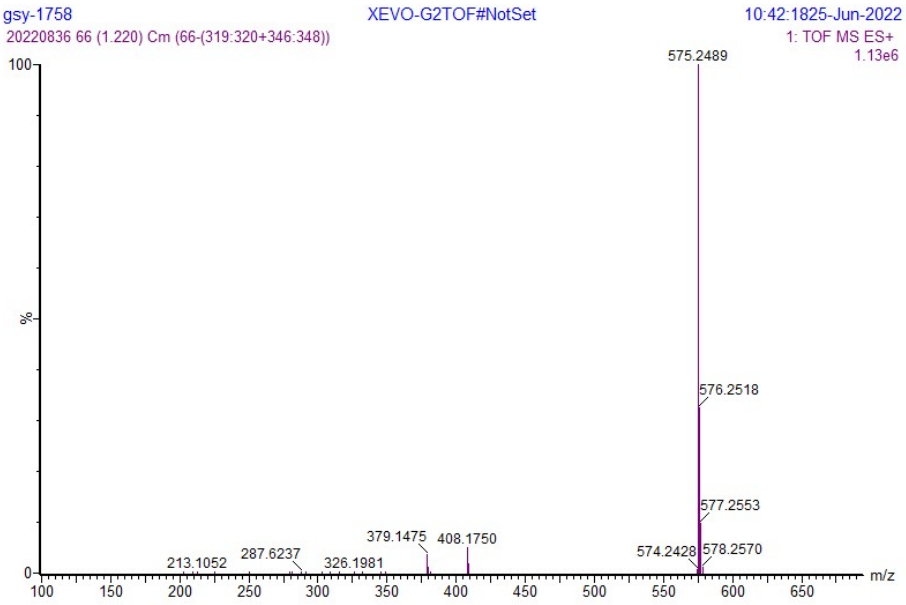

Fig. S22 The MS of TPA1.

Reference

[1] J. Xu, H. Liu, J. Li, Z. Zhao and B. Tang. *Adv. Optical Mater.* 2021, **9**, 2001840.

[2] C. Zheng, W. Zhao, Z. Wang, D. Huang, J. Ye, X. Ou, X. Zhang, C. Lee and S. Lee. *J. Mater. Chem.*, 2010, **20**, 1560-1566.

[3] S. Wang, M. Qiao, Z. Ye, D. Dou, M. Chen, Y. Peng, Y. Shi, X. Yang, L. Cui, J. Li, C. Li, B. Wei and W. Y. Wong. *iScience*, 2018, **9**, 532-541.

[4] F. Huang, H. Liu, W. Sun, X. Li and S. Wang. *J. Mater. Chem. C*, 2020, **8**, 9184-9188.

[5] C. Li, J. Wei, J. Han, Z. Li, X. Song, Z. Zhang, J. Zhang and Y. Wang. *J. Mater. Chem. C*, 2016, **4**, 10120-10129.

[6] J. Zhao, B. Liu, Z. Wang, Q. Tong, X. Du, C. Zheng, H. Lin, S. Tao and X. Zhang. *ACS Appl. Mater. Interfaces*, 2018, **10**, 9629-9637.

[7] X. Qiu, S. Ying, C. Wang, M. Hanif, Y. Xu, Y. Li, R. Zhao, D. Hu, D. Ma and Y. Ma. *J. Mater. Chem. C*, 2019,**7**, 592-600.

[8] W. Li, L. Yao, H. Liu, Z. Wang, S. Zhang, R. Xiao, H. Zhang, P. Lu, B. Yang and Y. Ma. *J. Mater. Chem. C*, 2014, **2**, 4733-4736.

[9] W. Qu, Z. Gao, W. Li, X. Fan, Y. Shi, Y. Miao, G. Yu, H. Zhou, J. Huang and H. Wang. *Dyes and Pigments*, 2021, **196**, 109808.

[10] X. Liu, H. Ge, Y. Zhao, D. Zhao, J. Fan and L. Liao. *J. Mater. Chem. C*, 2018, **6**, 4300-4307.

[11] W. Li, J. Li, D. Liu, D. Li and D. Zhang. *Chem. Sci.*, 2016, **7**, 6706-6714.

[12] J. Seo, S. Park, M. Kim, M. Suh and J. Lee. *Dyes and Pigments*, 2019, **162**, 959-

966.

[13] W. Li, J. Li, D. Liu, D. Li, and F. Wang. *ACS Appl. Mater. Interfaces*, 2016, **8**, 21497-21504.

[14] H. Zhou, M. Yin, Z. Zhao, Y. Miao, X. Jin, J. Huang, Z. Gao, H. Wang, J. Su and H. Tian. *J. Mater. Chem. C*, 2021, **9**, 5899-5907.

[15] K. Vadagaonkar, C. Yang, W. Zeng, J. Chen, B. Patil, P. Chetti, L. Chen and A. Chaskar. *Dyes and Pigments*, 2019, **160**, 301-314.